ACS Medicinal Chemistry Letters

Letter

pubs.acs.org/acsmedchemlett

Positron Emission Tomography to Elucidate Pharmacokinetic Differences of Regioisomeric Retinoid X Receptor Agonists

Toshiki Kobayashi,[†] Yuki Furusawa,[†] Shoya Yamada,[†,‡] Masaru Akehi,[§] Fumiaki Takenaka,[§] Takanori Sasaki,[§] Akiya Akahoshi,[§] Takahisa Hanada,[§] Eiji Matsuura,[§] Hiroyuki Hirano,[∥] Akihiro Tai,[⊥] and Hiroki Kakuta*[,†]

[†]Division of Pharmaceutical Sciences, Okayama University Graduate School of Medicine, Dentistry and Pharmaceutical Sciences, 1-1-1, Tsushima-Naka, Kita-ku, Okayama 700-8530, Japan

[‡]Research Fellowship Division, Japan Society for the Promotion of Science, Sumitomo-Ichibancho FS Bldg., 8 Ichibancho, Chiyoda-ku, Tokyo 102-8472, Japan

[§]Collaborative Research Center for OMIC, Okayama University Graduate School of Medicine, Dentistry and Pharmaceutical Sciences, 2-5-1 Shikata-Cho, Kita-ku, Okayama 700-8558, Japan

[∥]SHI Accelerator Service Ltd. 1-17-6 Osaki, Shinagawa-ku, Tokyo 141-0032, Japan

[⊥]Faculty of Life and Environmental Sciences, Prefectural University of Hiroshima, 562 Nanatsuka-Cho, Shobara, Hiroshima 727-0023, Japan

Supporting Information

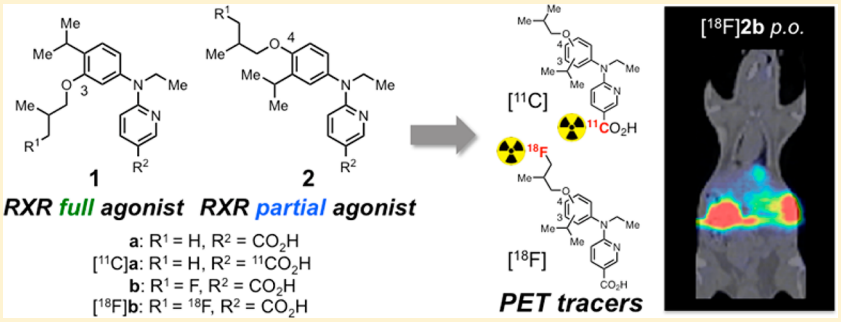

ABSTRACT: RXR partial agonist NEt-4IB (**2a**, 6-[ethyl-(4-isobutoxy-3-isopropylphenyl)amino]pyridine-3-carboxylic acid: EC_{50} = 169 nM, E_{max} = 55%) showed a blood concentration higher than its E_{max} after single oral administration at 30 mg/kg to mice, and repeated oral administration at 10 mg/kg/day to KK-A^y mice afforded antitype 2 diabetes activity without the side effects caused by RXR full agonists. However, RXR full agonist NEt-3IB (**1a**), in which the isobutoxy and isopropyl groups of **2a** are interchanged, gave a much lower blood concentration than **2a**. Here we used positron emission tomography (PET) with tracers [^{11}C]**1a**, [^{11}C]**2a** and fluorinated derivatives [^{18}F]**1b**, [^{18}F]**2b**, which have longer half-lives, to examine the reason why **1a** and **2a** exhibited significantly different blood concentrations. As a result, the reason for the high blood concentration of **2a** after oral administration was found to be linked to higher intestinal absorbability together with lower biliary excretion, compared with **1a**.

KEYWORDS: *Nuclear receptors, RXR, PET imaging, pharmacokinetics*

Bexarotene (EC_{50} = 20 nM, E_{max} = 100%) (Figure 1), a retinoid X receptor (RXR) agonist, is clinically used for the treatment of cutaneous T cell lymphoma (CTCL) in the United States[1] and is also reported to show curative effects on type-2 diabetes,[2] Alzheimer's disease,[3] and Parkinson's disease[4] in animal models. However, experience with RXR full agonists, including bexarotene, has shown that they can cause serious adverse effects, including hypothyroidism, hepatomegaly, weight gain, and elevation of blood triglyceride.[5−9] Aiming to create new RXR agonists without these side effects, we have designed, synthesized, and characterized RXR full agonist NEt-3IB (**1a**: 6-[ethyl-(3-isobutoxy-4-isopropylphenyl)amino]-pyridine-3-carboxylic acid)[10,11] and RXR partial agonist NEt-4IB (**2a**: 6-[ethyl-(4-isobutoxy-3-isopropylphenyl)amino]-pyridine-3-carboxylic acid)[12] (Figure 1). Compound **1a** was designed by introducing a polar alkoxy group into the hydrophobic moiety to lower the lipophilicity because previous RXR agonists including bexarotene are quite lipophilic. However, **2a** was obtained as a RXR partial agonist based on the hypothesis that RXR partial agonists, which only partially

Received: December 8, 2014
Accepted: January 20, 2015

ACS Publications © XXXX American Chemical Society

DOI: 10.1021/ml500511m
ACS Med. Chem. Lett. XXXX, XXX, XXX−XXX

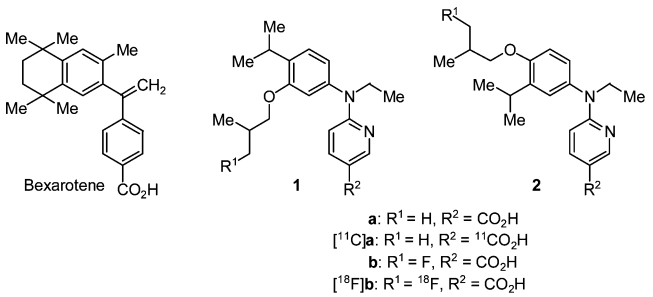

Figure 1. Chemical structures of RXR full agonists bexarotene and **1**, and RXR partial agonist **2**.

activate RXR, might have minimal side effects since the reported adverse effects are associated primarily with RXR full agonists that maximally activate RXRs. Oral administration of RXR partial agonist **2a** gave a considerably higher blood concentration (AUC = 18.8 h·mg/L at 30 mg/kg, *p.o.*) than that of **1a** (AUC = 1.14 h·mg/L at 30 mg/kg, *p.o.*), and indeed, **2a** showed a potent glucose-lowering effect in type 2 diabetes model mice without inducing serious adverse effects.[12] Since **1a** is a regioisomer of **2a** and its hydrophobic moiety was constructed simply by interchanging the isobutoxy and isopropyl groups of **1a**, we were interested in the reason for the significant pharmacokinetic difference between **1a** and **2a**.

The blood concentration of a drug is determined by the balance of intestinal absorption, distribution, metabolism, and excretion. To examine the pharmacokinetics of **1a** and **2a** *in vivo*, we aimed to employ positron emission tomography (PET). PET imaging can be performed noninvasively and sequentially, that is, the target compound does not need to be extracted, and its distribution can be detected with high resolution.[13,14] Moreover, since PET-based pharmacokinetic studies of bexarotene have been reported,[15] it would be of interest to compare the results for **1a** or **2a** with the reported data for bexarotene. PET imaging requires appropriate labeling of the target compounds, for example, with ^{11}C or ^{18}F. Therefore, we synthesized [^{11}C]**1a** and [^{11}C]**2a**, which possess an ^{11}C carboxylic acid moiety, and the ^{18}F derivatives 6-{ethyl-[3-(3-fluoro-2-methylpropoxy)-4-isopropylphenyl]amino}-nicotinic acid ([^{18}F]**1b**) and 6-{ethyl-[3-(3-fluoro-2-methylpropoxy)-4-isopropylphenyl]amino}nicotinic acid ([^{18}F]**2b**) (Figure 1) as PET tracers for the present imaging analyses.

[^{11}C]**1a** and [^{11}C]**2a** were synthesized according to Supporting Information (SI) Scheme 1. The coupling reactions of **3** and **4** with **5** gave **6** and **7**, and *N*-ethylation at the linking amino atom afforded **8** and **9**, respectively. Lithiation of **8** and **9** was performed by the addition of an ether solution of each compound at −78 °C via a syringe into the reaction vessel of an automated reaction chamber, which contained *n*-BuLi in dry ether at −20 °C (the lowest temperature setting of the apparatus).[16] After the lithiation, $^{11}CO_2$ was bubbled into the reaction vessel, and then excess base was neutralized with *p*-toluenesulfonic acid (*p*-TSA) to give [^{11}C]**1a** and [^{11}C]**2a**, respectively. HPLC analysis revealed that these products showed the same retention times as the corresponding unlabeled compounds. The radioactive purity was 99.2% and 98.6% (SI Charts S3 and S4), and the yield of radioactivity from $^{11}CO_2$ was 2.0% (1.75 GBq) and 0.45% (167 MBq), respectively.

Compounds **1b** and **2b** were synthesized from **12** and **13**, respectively,[10−12] which have already been reported as precursors of **1a** and **2a** (SI Scheme 2). Removal of the isopropyl group of **12** and **13** by using $AlCl_3$ afforded **14** and **15**, respectively. These compounds were reacted with **11** to afford **16** and **17**, respectively. Catalytic reduction using Pd/C failed to remove the benzyl protection, but the use of $AlCl_3$ afforded **18** and **19**, and the hydroxyl group was converted to a triflate group to afford **20** and **21**, respectively. The nonradioactive [^{19}F] compounds were synthesized according to the synthetic scheme for fluorodeoxyglucose (FDG);[17] fluorination was performed by the reaction of **20** or **21** with KF in a mixture of Kryptofix 222 and K_2CO_3 in MeCN at 90 °C. Then, after hydrolysis of the ester group with $NaOH_{aq}$, neutralization with hydrochloric acid on an ice bath gave **1b** and **2b**, respectively. The [^{18}F] derivatives were obtained similarly, except for the use of [^{18}F]KF and neutralization after hydrolysis of the ester. Neutralization after hydrolysis was performed by using *p*-TSA in MeOH instead of hydrochloric acid, to ensure compatibility with the eluent used for preparative chromatography ($AcONH_{4aq}$/MeOH = 20:80). After preparative chromatography, [^{18}F]**1b** and [^{18}F]**2b** showed the same retention times as the corresponding **1b** and **2b**. The radioactive purity was 98.5% and 99.6% (SI Charts S5 and S6), and the yield of radioactivity from ^{18}F was 18% (6.2 GBq) and 10% (3.4 GBq), respectively.

Since it is reported that introduction of a fluorine atom decreases the hydrophobicity of the original compound,[18] the polarity and RXRα-agonistic activity of **1b** and **2b** were examined. Both HPLC retention times were shortened by about 5 min, but the order of polarity was maintained (Table 1). Evaluation of RXRα-agonistic activities using luciferase

Table 1. HPLC Retention Time and Luciferase Reporter Gene Assay Data of Each Compound[a]

		RXRα	
	retention time (min)	E_{max} (%)	EC_{50} (nM)
1a	12.7	114 ± 0	19 ± 6
1b	7.63	98 ± 5	12 ± 3
2a	11.7	55 ± 2	169 ± 3
2b	6.70	52 ± 5	450 ± 30

[a]Conditions: HPLC analyses were performed by using an Inertsil ODS-3 column (4.6 i.d. × 100 mm, 3 μm, GL Sciences, Tokyo, Japan). The flow rate was 0.7 mL/min with methanol/25 mM ammonium acetate (adjusted with acetic acid to pH 5.0) (80:20 v/v) as the mobile phase. The UV absorbance was monitored at 260 nm. Luciferase activity of bexarotene at 1 μM was defined as 100%. EC_{50} values were determined from full dose−response curves in COS-1 cells. Data shown are the average (n = 4−5) ± SEM.

transcription assay in COS-1 cells revealed that compounds **1b** and **2b** showed full RXRα-agonistic activity and partial RXRα-agonistic activity, respectively, like **1a** and **2a** (Table 1). While the addition of a fluorine atom in going from **1a** to **1b** did not greatly affect the EC_{50}, the addition of a fluorine atom in going from **2a** to **2b** had a more profound effect on the EC_{50}. A possible explanation of this difference is that small perturbations in potent agonists do not exhibit as large binding/activation effects as small perturbations in partial agonists.

Each PET tracer was dissolved in EtOH and then diluted with saline to 10 MBq, and the diluted solution was administered to mice. Then, PET scanning was performed for 30 min. The data were reconstructed at selected times, and the radioactivity of the whole body and each organ of the mice was

DOI: 10.1021/ml500511m
ACS Med. Chem. Lett. XXXX, XXX, XXX−XXX

calculated in Bq. The pharmacokinetics using each tracer was compared in terms of the percentage of injected dose (%ID) values, i.e., the radioactivity of each organ (Bq) per the radioactivity of the whole body (Bq).

To compare the time dependency of the blood concentration of each compound, radioactivity in blood was calculated as % ID/mL by dividing the %ID value in the heart by the heart volume (Figures 2a,b and SI Figure S1a). The AUC values from

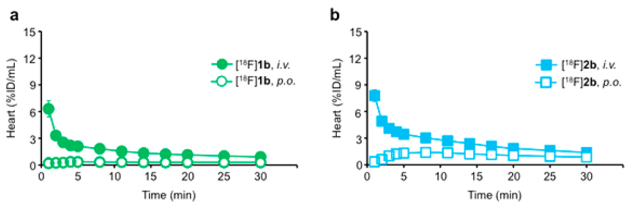

Figure 2. Real-time changes in region of interest (ROI) of the PET images with [^{18}F]**1b** (closed or open green circle) and [^{18}F]**2b** (closed or open blue squares). Time course of (a) [^{18}F]**1b** administered *p.o.* or *i.v.* and (b) [^{18}F]**2b** administered *p.o.* or *i.v.* were obtained from the mean pixel radioactivity in the ROI of the PET images acquired after administration. Data shown are the average (n = 3−5) ± SEM.

time 0 to 30 min for [^{18}F]**1b** and [^{18}F]**2b** after intravenous injection were 17 h·%ID/mL and 27 h·%ID/mL, respectively. The [^{11}C] derivatives gave similar results (SI Figure S1a). Since ^{18}F has a longer half-time than ^{11}C, subsequent PET analyses were performed with [^{18}F]**1b** or [^{18}F]**2b**. AUC values after oral administration were 3.1 h·%ID/mL for [^{18}F]**1b** and 12 h·%ID/mL for [^{18}F]**2b**. The AUC ratio of [^{18}F]**2b** to [^{18}F]**1b** was about 1.6-fold for intravenous injection and about 4-fold for oral administration. Thus, the difference of blood concentration after oral administration of each compound is thought to be due to, at least in part, different gastrointestinal absorption characteristics. The bioavailability was calculated as the ratio of dose-corrected AUC after oral administration to that after intravenous injection, and 0.18 for [^{18}F]**1b** and 0.43 for [^{18}F]**2b**, indicating that [^{18}F]**2b** is preferable for oral administration. In the case of intravenous injection, the difference of blood concentration between the two compounds would be due to a difference of distribution or excretion. Therefore, it is suggested that the difference of blood concentration between the two regioisomers in the case of oral administration may be a consequence of differences in intestinal absorption, distribution, and excretion.

To examine the intestinal absorption, distribution, and excretion of each compound macroscopically, the PET/CT images after administration of each PET tracer were compared (SI Figure S2). In the case of intravenous injection, both tracers initially moved into the heart, followed by the liver, and then were distributed to the gallbladder and the duodenum. The radioactivity in the kidney or the urinary bladder was markedly lower than in the liver or gallbladder. These findings suggested that both tracers are excreted mainly from the gallbladder, rather than from the kidney. In the case of oral administration, each compound was accumulated in the stomach first and then moved to the duodenum. After intestinal absorption, the compounds were distributed to the liver, moved to the gallbladder, and excreted via the duodenum. The tracers were still detected in the stomach at the end of the scanning period (after 30 min). The radioactivity of each compound in the kidney or urinary bladder was lower than in the gallbladder, suggesting that these compounds are predominantly excreted via the biliary route. In addition, both compounds exhibited enterohepatic circulation, being reabsorbed from the small intestine, taken up by enterocytes and transported back to the liver (SI Movies S1 and S2).

To compare the pharmacokinetics in detail, the radioactivity in each organ was quantified. Regions of interest (ROIs) were defined using PET/CT imaging data and the radioactivity (% ID) at each organ at each time was calculated (Figure 3 and SI

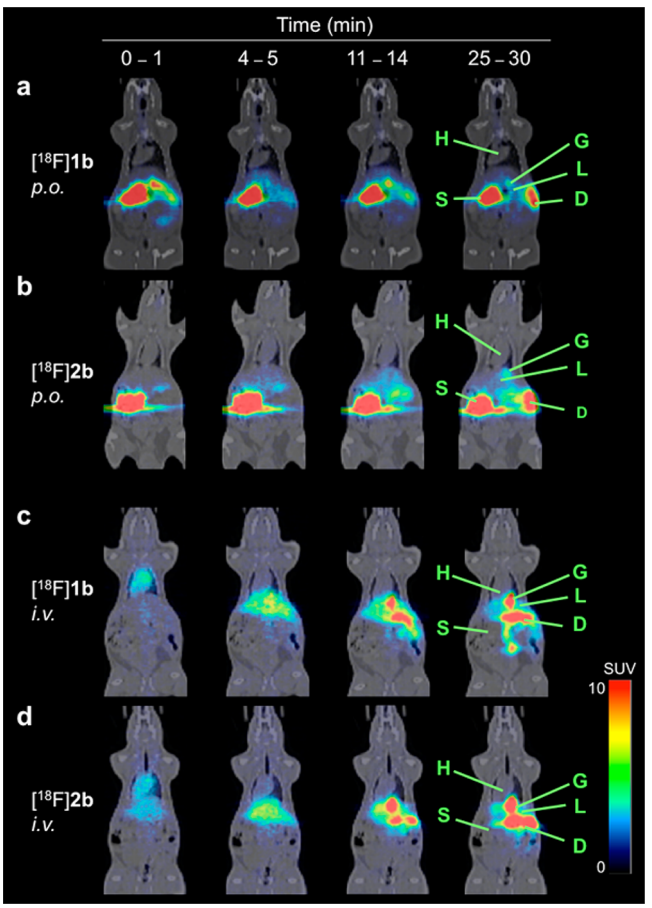

Figure 3. Decay-corrected whole-body coronal PET/CT images of mice from static scans at 0−1, 4−5, 11−14, and 25−30 min after administration of [^{18}F]**1b** or [^{18}F]**2b**. (a) [^{18}F]**1b** *p.o.*; (b) [^{18}F]**2b** *p.o.*; (c) [^{18}F]**1b** *i.v.*; (d) [^{18}F]**2b** *i.v.*; H, S, G, L, and D indicate heart, stomach, gallbladder, liver, and duodenum, respectively.

Figure S3). However, radioactivity (%ID) in the kidneys could not be evaluated because the organ was located too close to the stomach and duodenum. The %ID of [^{18}F]**2b** at each organ tended to be higher than that of [^{18}F]**1b** by a ratio that was proportional to the difference of blood concentration. In particular, lung and muscle showed a marked difference in the case of intravenous injection. Focusing on the %ID at the liver after intravenous injection, [^{18}F]**1b** gave a higher value than [^{18}F]**2b**, contrary to the order of blood concentration (Figure 4h). Since the compounds were administered at the same dosage, [^{18}F]**1b** was thought to migrate more easily to the liver than [^{18}F]**2b**. Measurement of radioactivity at the gallbladder revealed that [^{18}F]**1b** gave a significantly higher value than [^{18}F]**2b**, similarly to the case of liver after intravenous injection (Figure 4e,f). Similar results were obtained with the [^{11}C] tracers (SI Figure S1). Thus, the difference of blood concentration appears to be at least partly due to a difference

DOI: 10.1021/ml500511m
ACS Med. Chem. Lett. XXXX, XXX, XXX−XXX

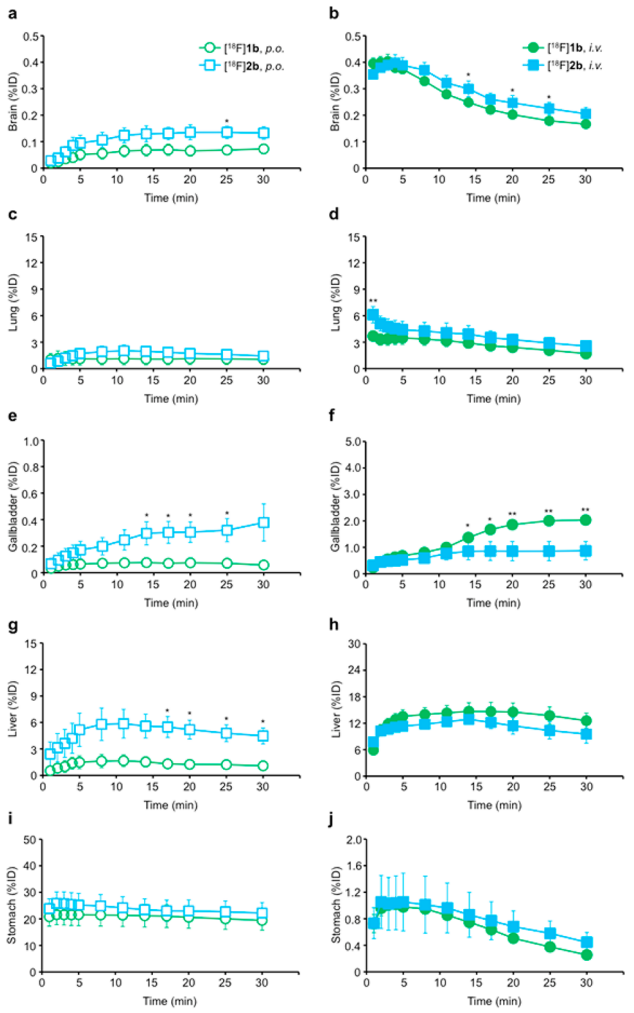

Figure 4. Real-time changes in the ROI of the PET images with [^{18}F]**1b** (open or closed green circle) and [^{18}F]**2b** (open or closed blue squares). Time course of %ID (a) brain *p.o.*, (b) brain *i.v.*, (c) lung *p.o.*, (d) lung *i.v.*, (e) gallbladder *p.o.*, (f) gallbladder *i.v.*, (g) liver *p.o.*, (h) liver *i.v.*, (i) stomach *p.o.*, and (j) stomach *i.v.* were obtained from the mean pixel radioactivity in ROI of the PET images acquired with frames after the administration. Data shown are the average (n = 3–5) ± SEM and analyzed by one-way ANOVA followed by t-test. Significant differences: *p < 0.05, **p < 0.01 vs [^{18}F]**2b**.

of biliary excretion after hepatic metabolism. According to Lipinsky's rule, properties that would make a drug a likely candidate for oral administration in humans include logP lower than 5, because highly hydrophobic compounds tend to be poorly absorbed after oral administration.[19] The HPLC results support the idea that **1a**,**b** are less polar than **2a**,**b**, and this may influence the oral absorption. Moreover, the greater hydrophobicity of **1a**,**b** than **2a**,**b** may favor transfer to the liver and biliary excretion. With both tracers, the %ID of the urinary bladder is lower than that of the gallbladder, indicating that these compounds are poorly excreted from the kidney (SI Figure S2g,h). The predominant biliary excretion of these compounds may make them good candidates for treatment of patients with impaired renal function.

Next, we compared the %ID values of the two compounds in the stomach, upper digestive tract, and lower digestive tract after oral administration (Figure 4i,j and SI Figure S2a–d). The radioactivity in the stomach or upper digestive tract after oral administration of each regioisomer was higher than that in the lower digestive tract, and there was no difference between the regioisomers. The reason for this may be inhibition of peristaltic movement by anesthesia.[20] Enterohepatic circulation may also restrict transfer of the compounds to the lower digestive tract.

Brain uptake of each tracer was observed by PET after intravenous injection, as well as oral administration (Figure 4a,b and SI Figure S1b). These results are similar to those reported for [^{11}C]bexarotene administered to a baboon, *Papio anubis*,[15] though it is important to note that there are very likely to be species differences in bexarotene behavior. The blood concentrations of nonradioactive bexarotene, **1a**, and **2a** at 1 h after single oral administration of 30 mg/kg in 0.5% CMC suspensions to mice were 4150, 1320, and 6760 ng/mL, respectively (SI Table S1). The brain concentrations of bexarotene and **1a** were 1960 and 978 ng/mL, respectively, whereas that of **2a** is 2570 ng/mL. These results are consistent with the PET analysis data. The brain-to-blood concentration ratios of bexarotene, **1a**, and **2a** were 0.47, 0.74 and 0.38, respectively. Although the brain concentration of bexarotene seems lower than that reported by Landreth et al.,[21] this may be due to the different suspension formulations employed. Since the lipophilicity of **1a** is higher than that of **2a** as shown by HPLC and more lipophilic compounds can be transported through the blood–brain barrier more easily, the above results may reflect the differences of lipophilicity of the compounds. However, since the blood concentration of **2a** was higher than that of **1a**, more **2a** was transported into the brain, as compared to **1a**.

In conclusion, PET imaging data revealed that **2a**,**b** are absorbed more easily from the digestive tract and excreted more slowly than **1a**,**b**. The brain concentrations of **2a**,**b** were markedly higher than those of **1a**,**b**. Thus, the partial RXR agonist **2a** appears to be a promising candidate for the treatment of Alzheimer's and Parkinson's diseases without the serious side effects caused by RXR full agonists such as bexarotene. Both compounds show predominantly biliary excretion, which would be favorable in the treatment of patients with impaired renal function.

■ ASSOCIATED CONTENT

Ⓢ Supporting Information

Supplementary *in vitro* and *in vivo* data. This material is available free of charge via the Internet at http://pubs.acs.org.

■ AUTHOR INFORMATION

Corresponding Author

*Tel/Fax: +81-(0)86-251-7963. E-mail: kakuta-h@cc.okayama-u.ac.jp.

Author Contributions

H.K. conceived and designed the project. T.K. synthesized compounds. T.K. and S.Y. performed reporter gene assays. T.K., Y.F., and H.K. performed in vivo experiments. T.K., F.T., M.A., H.H., and H.K. synthesized PET tracers. T.S., A.A., and T.H., performed PET scanning. T.K., A.T., and H.K. performed HPLC analysis. The manuscript was written by T.K., E.M., A.T., and H.K.

Funding

This work was supported by a subsidy to promote science and technology in prefectures where nuclear and other power plants

DOI: 10.1021/ml500511m
ACS Med. Chem. Lett. XXXX, XXX, XXX–XXX

are located (to H.K.) from the Ministry of Education, Culture, Sports, Science and Technology (MEXT) of Japan.

Notes

The authors declare no competing financial interest.

■ ACKNOWLEDGMENTS

The authors are grateful to Prof. Yoshio Naomoto, Dr. Takuya Fukazawa (Kawasaki Medical School), Dr. Kaori Endo-Umeda (Nihon University), and Prof. Makoto Makishima (Nihon University) for preparing plasmids. The authors are grateful to the Division of Instrumental Analysis, Okayama University for the NMR measurements.

■ ABBREVIATIONS

RXR, retinoid X receptor; PET, positron emission tomography; E_{max}, maximum efficacy; EC_{50}, half-maximal (50%) effective concentration; *p*-TSA, *p*-toluenesulfonic acid; SEM, standard error of the mean; ROI, region(s) of interest; SUV, standard uptake values; EOB, end of bombardment; CMC, carboxymethyl cellulose

■ REFERENCES

(1) Pileri, A.; Delfino, C.; Grandi, V.; Pimpinelli, N. Role of bexarotene in the treatment of cutaneous T-cell lymphoma: the clinical and immunological sides. *Immunotherapy* **2013**, *5*, 427−433.

(2) Mukherjee, R.; Davies, P. J.; Crombie, D. L.; Bischoff, E. D.; Cesario, R. M.; Jow, L.; Hamann, L. G.; Boehm, M. F.; Mondon, C. E.; Nadzan, A. M.; Paterniti, J. R., Jr.; Heyman, R. A. Sensitization of diabetic and obese mice to insulin by retinoid X receptor agonists. *Nature* **1997**, *386*, 407−410.

(3) Cramer, P. E.; Cirrito, J. R.; Wesson, D. W.; Lee, C. Y.; Karlo, J. C.; Zinn, A. E.; Casali, B. T.; Restivo, J. L.; Goebel, W. D.; James, M. J.; Brunden, K. R.; Wilson, D. A.; Landreth, G. E. ApoE-directed therapeutics rapidly clear *β*-amyloid and reverse deficits in AD mouse models. *Science* **2012**, *335*, 1503−1506.

(4) McFarland, K.; Spalding, T. A.; Hubbard, D.; Ma, J. N.; Olsson, R.; Burstein, E. S. Low dose bexarotene treatment rescues dopamine neurons and restores behavioral function in models of Parkinson's disease. *ACS Chem. Neurosci.* **2013**, *4*, 1430−1438.

(5) Sherman, S. I. Etiology, diagnosis, and treatment recommendations for central hypothyroidism associated with bexarotene therapy for cutaneous T-cell lymphoma. *Clin. Lymphoma* **2003**, *3*, 249−252.

(6) Lenhard, J. M.; Lancaster, M. E.; Paulik, M. A.; Weiel, J. E.; Binz, J. G.; Sundseth, S. S.; Gaskill, B. A.; Lightfoot, R. M.; Brown, H. R. The RXR agonist LG100268 causes hepatomegaly, improves glycaemic control and decreases cardiovascular risk and cachexia in diabetic mice suffering from pancreatic beta-cell dysfunction. *Diabetologia* **1999**, *42*, 545−554.

(7) Standeven, A. M.; Escobar, M.; Beard, R. L.; Yuan, Y. D.; Chandraratna, R. A. Mitogenic effect of retinoid X receptor agonists in rat liver. *Biochem. Pharmacol.* **1997**, *54*, 517−524.

(8) Standeven, A. M.; Thacher, S. M.; Yuan, Y. D.; Escobar, M.; Vuligonda, V.; Beard, R. L.; Chandraratna, R. A. Retinoid X receptor agonist elevation of serum triglycerides in rats by potentiation of retinoic acid receptor agonist induction or by action as single agents. *Biochem. Pharmacol.* **2001**, *62*, 1501−1509.

(9) de Vries-van der Weij, J.; de Haan, W.; Hu, L.; Kuif, M.; Oei, H. L.; van der Hoorn, J. W.; Havekes, L. M.; Princen, H. M.; Romijn, J. A.; Smit, J. W.; Rensen, P. C. Bexarotene induces dyslipidemia by increased very low-density lipoprotein production and cholesteryl ester transfer protein-mediated reduction of high-density lipoprotein. *Endocrinology* **2009**, *150*, 2368−2375.

(10) Takamatsu, K.; Takano, A.; Yakushij, N.; Morohashi, K.; Morishita, K.; Matsuura, N.; Makishima, M.; Tai, A.; Sasaki, K.; Kakuta, H. The first potent subtype-selective retinoid X receptor (RXR) agonist possessing a 3-isopropoxy-4-isopropylphenylamino moiety, NEt-3IP (RXR*α*/*β*-dual agonist). *ChemMedChem* **2008**, *3*, 780−787.

(11) Ohsawa, F.; Morishita, K.; Yamada, S.; Makishima, M.; Kakuta, H. Modification at the lipophilic domain of RXR agonists differentially influences activation of RXR heterodimers. *ACS Med. Chem. Lett.* **2010**, *1*, 521−525.

(12) Kawata, K.; Morishita, K.; Nakayama, M.; Yamada, S.; Kobayashi, T.; Furusawa, Y.; Arimoto-Kobayashi, S.; Oohashi, T.; Makishima, M.; Naitou, H.; Ishitsubo, E.; Tokiwa, H.; Tai, A.; Kakuta, H. RXR partial agonist produced by side chain repositioning of alkoxy RXR full agonist retains antitype 2 diabetes activity without the adverse effects. *J. Med. Chem.* **2014**, x DOI: 10.1021/jm501863r.

(13) Bergström, M.; Grahnen, A.; Långström, B. Positron emission tomography microdosing: a new concept with application in tracer and early clinical drug development. *Eur. J. Clin. Pharmacol.* **2003**, *59*, 357−366.

(14) Fischman, A. J.; Alpert, N. M.; Rubin, R. H. Pharmacokinetic imaging: a noninvasive method for determining drug distribution and action. *Clin. Pharmacokinet.* **2002**, *41*, 581−602.

(15) Rotstein, B. H.; Hooker, J. M.; Woo, J.; Collier, T. L.; Brady, T. J.; Liang, S. H.; Vasdev, N. Synthesis of [^{11}C]bexarotene by Cu-mediated [^{11}C]carbon dioxide fixation and preliminary PET imaging. *ACS Med. Chem. Lett.* **2014**, *6*, 668−672.

(16) Van der Mey, M.; Janssen, C. G.; Janssens, F. E.; Jurzak, M.; Langlois, X.; Sommen, F. M.; Verreet, B.; Windhorst, A. D.; Leysen, J. E.; Herscheid, J. D. Synthesis and biodistribution of [(11)C]R116301, a promising PET ligand for central NK(1) receptors. *Bioorg. Med. Chem.* **2005**, *13*, 1579−1586.

(17) Hamacher, K.; Coenen, H. H.; Stocklin, G. Efficient stereospecific synthesis of no-carrier-added 2-[^{18}F]-fluoro-2-deoxy-D-glucose using aminopolyether supported nucleophilic substitution. *J. Nucl. Med.* **1986**, *27*, 235−238.

(18) Böhm, H. J.; Banner, D.; Bendels, S.; Kansy, M.; Kuhn, B.; Müller, K.; Obst-Sander, U.; Stahl, M. Fluorine in medicinal chemistry. *ChemBioChem* **2004**, *5*, 637−643.

(19) Lipinski, C. A.; Lombardo, F.; Dominy, B. W.; Feeney, P. J. Experimental and computational approaches to estimate solubility and permeability in drug discovery and development settings. *Adv. Drug Delivery Rev.* **2001**, *46*, 3−26.

(20) Yamashita, S.; Takashima, T.; Kataoka, M.; Oh, H.; Sakuma, S.; Takahashi, M.; Suzuki, N.; Hayashinaka, E.; Wada, Y.; Cui, Y.; Watanabe, Y. PET imaging of the gastrointestinal absorption of orally administered drugs in conscious and anesthetized rats. *J. Nucl. Med.* **2011**, *52*, 249−256.

(21) Landreth, G. E.; Cramer, P. E.; Lakner, M. M.; Cirrito, J. R.; Wesson, D. W.; Brunden, K. R.; Wilson, D. A. Response to comments on "ApoE-directed therapeutics rapidly clear *β*-amyloid and reverse deficits in AD mouse models". *Science* **2013**, *340*, 924−g.

DOI: 10.1021/ml500511m
ACS Med. Chem. Lett. XXXX, XXX, XXX−XXX